

# Recipe for Intensity Modulation Reduction in SOA-Based Interferometric Switches

Nikos Pleros, *Student Member, IEEE*, Chris Bintjas, George T. Kanellos, Kyriakos Vlachos, *Member, IEEE*, Hercules Avramopoulos, and George Guekos, *Member, IEEE, Member, OSA*

**Abstract**—This paper presents a theoretical and experimental analysis of saturated semiconductor optical amplifier (SOA)-based interferometric switching arrangements. For the first time, it is shown that such devices can provide enhanced intensity modulation reduction to return-to-zero (RZ) formatted input pulse trains, when the SOA is saturated with a strong continuous-wave (CW) input signal. A novel theoretical platform has been developed in the frequency domain, which reveals that the intensity modulation of the input pulse train can be suppressed by more than 10 dB at the output. This stems from the presence of the strong CW signal that transforms the sinusoidal transfer function of the interferometric switch into an almost flat, strongly nonlinear curve. This behavior has also been verified experimentally for both periodically and randomly degraded, in terms of intensity modulation, signals at 10 Gb/s using the ultrafast nonlinear interferometer as the switching device. Performance analysis both in the time and frequency domains is demonstrated, verifying the concept and its theoretical analysis.

**Index Terms**—All-optical signal processing, intensity modulation, interferometric switches, nonlinear transfer function, optical packet switching, optical regeneration, semiconductor optical amplifier (SOA), wavelength conversion.

## I. INTRODUCTION

WHILE raw point-to-point transmission capacity has increased dramatically in the past years, the advantages offered from it still cannot be fully exploited as the performance of switching and processing technology still lags behind [1]. This has pushed efforts toward the implementation of optical devices, subsystems, and network architectures that will be able to handle high-data-rate optical signals. Within this frame, significant research effort has been invested in all-optical switching and signal processing techniques. As such, highly improved, optically controlled, high-speed interferometric arrangements [2]–[4] have emerged and have been used in hero experiments [5]–[8].

The maturity of semiconductor technology has contributed to this effort [2], [4] and lead to a whole new class of compact circuits that can be potentially integrated on a chip module [9], [10]. To this end, the deployment of high-speed optical gates allowed for the demonstration of key functionalities such as bit-wise Boolean logic [8], [10], [11], demultiplexing [12], [13],

wavelength conversion [7], [14]–[16], regeneration [5], [17], [18] and data processing and routing [19], [20], directly in the optical domain. The speed advantage of these devices mainly owes to the exploitation of the ultrafast cross-phase modulation (XPM) phenomenon in semiconductor optical amplifiers (SOAs).

Despite these achievements, it is doubtful whether the potential of SOA-based optical switches, in terms of improved performance characteristics and their contribution to the realization of key network functionalities, has been fully utilized. Several techniques such as the optical holding beam technique [21] and optical pumping at transparency [22]–[24] have been proposed for enhancing the switching capabilities of already developed technology, emphasizing its speed characteristics. Recently, we have proposed the use of deeply saturated optical gates to demonstrate a clock recovery circuit ideal for short optical packets [25], even in the asynchronous traffic regime [26]. This work has indicated that SOA-based optical gates can offer improved pulse amplitude equalization characteristics under certain operational conditions; however, no detailed analysis has been presented so far. This novel circuit has also lead to the demonstration of several functional subsystems for optical packet switching applications [27]–[29].

In this paper, a detailed theoretical and experimental investigation of deeply saturated SOA-based interferometric gates is presented and, for the first time to the authors' knowledge, the improvement in the intensity modulation reduction (IMR) properties of such devices is shown. The theoretical model was developed based on the Mach-Zehnder interferometric (MZI) configuration using simplified analytical expressions for the semiconductor response [30], [31]. Analysis in the frequency domain revealed that the operation of the device in the deeply saturated regime, by means of a strong continuous-wave (CW) input signal, provides increased IMR to return-to-zero (RZ) input data signals, compared with the conventional mode of operation in low or moderate saturation. The output-versus-input-power transfer function of the device for several saturation levels of the amplifier is also examined in order to investigate this behavior. It is shown that as the saturation level of the SOA increases, the regular sinusoidal response of the interferometer transforms into an almost flat, strongly nonlinear curve. Following this analysis, experimental verification is provided for 10-Gb/s pulse sequences with both periodical and random intensity modulation, using a typical ultrafast nonlinear interferometer (UNI) switch. The experimental evaluation has been performed in the frequency and time domains and has shown good agreement with the theory.

Manuscript received September 17, 2003; revised June 28, 2004.

N. Pleros, C. Bintjas, G. T. Kanellos, and H. Avramopoulos are with the Department of Electrical and Computer Engineering, National Technical University of Athens, GR15773 Athens, Greece (e-mail: npleros@cc.ece.ntua.gr).

K. Vlachos is with Computer Engineering and Informatics Department, University of Patras, School of Engineering, GR-26500 Rio Patra, Greece.

G. Guekos is with the Swiss Federal Institute of Technology Zurich, ETH Hoenggerberg, CH-8093 Zurich, Switzerland.

Digital Object Identifier 10.1109/JLT.2004.834834

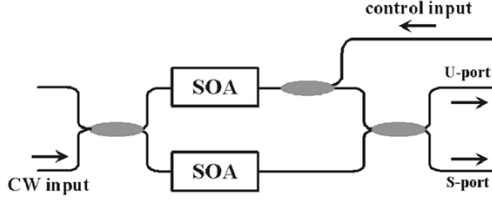


Fig. 1. MZI configuration.

It is therefore expected that this technique can offer improved regenerative properties, when applied to conventional wavelength conversion and switching schemes, or even lead to novel functional concepts for packet switching applications.

The remainder of the paper is organized as follows. Section II presents the theoretical analysis in detail, and Section III provides the experimental verification for both periodical and random intensity modulated 10-Gb/s pulsed signals. Finally, Section IV discusses the possible applications of the proposed scheme and outlines its advantages.

## II. THEORETICAL ANALYSIS

Fig. 1 depicts the basic elements of an SOA-based MZI switch arranged in a counterpropagating configuration. The interferometer consists of two separate optical paths, each one having an SOA as the nonlinear, optically controlled active element. The input signal is inserted into the gate and split into two spatial components via a 3-dB fiber coupler. Optically controlled operation of the switch is achieved by means of a second optical signal, hereinafter called the control signal, which is inserted into the upper branch SOA via a fiber coupler and propagates in the opposite direction of the input signal. For the purposes of our investigation, a CW signal and a pulsed optical beam are considered to be the input and the control signals in the switch, respectively, whereas the two SOAs are assumed to be two identical devices. The two CW components travel through the corresponding branches of the interferometer and recombine in a second 3-dB fiber coupler placed at the output. In this way, the two input CW signal parts are forced to interfere and, in the absence of any control pulse, the incoming input signal exits the gate through the one output port of the coupler, hereinafter called U-port (unswitched).

In the presence of a control pulse, the nonlinear interaction between the injected photons and the SOA carriers imposes a refractive-index change in the semiconductor. This is perceived by the CW signal component that temporally coincides with the control pulse in the SOA, as a phase variation, which in turn results in a total differential phase shift between the two CW spatial components. To this end, their interference at the output coupler forces part of the incoming CW power to emerge at the second port of the coupler, hereinafter called the S-port (switching), and the control signal is imprinted on the CW optical beam.

The following analysis aims to provide a theoretical insight into the switching mechanism of the gate in order to investigate the intensity modulation of the switched waveform, when an intensity modulated RZ pulse train is used as the control signal. Defining as  $P_{CW}$  the incoming CW signal power and, as  $G_1(t)$  and  $G_2(t)$  the power gains experienced by the CW signal in each

SOA in the upper and lower branch of the switch, respectively, the switched optical power at the S-output port is expressed as

$$P_S(t) = \frac{P_{CW}}{4} [G_1(t) + G_2(t) - 2\sqrt{G_1(t)G_2(t)} \cdot \cos(\Delta\varphi(t))]. \quad (1)$$

In (1),  $\Delta\varphi(t)$  represents the phase difference between the two CW components and is expressed as [31]

$$\Delta\varphi(t) = -\frac{\alpha}{2} \ln[G_1(t)/G_2(t)] \quad (2)$$

with  $\alpha$  denoting the linewidth enhancement factor of each SOA. For the adopted MZI configuration, the gain of the lower branch SOA  $G_2(t)$  will always remain in a time-independent equilibrium value, since there is no input for control signal injection available. This equilibrium value is determined by the CW input power and is below the SOA small-signal gain  $G_0$ . Considering the amplifier as a spatially concentrated device and following the approaches described in [21] and [30],  $G_2(t)$  is given by

$$G_2(t) = G_{CW} = G_0 \cdot \exp[-(G_{CW} - 1)P_{CW}/2P_{sat}] \quad (3)$$

where  $P_{sat}$  is the saturation power parameter of the SOA and  $P_{CW}/2$  represents the power of the CW signal component at the input of the lower branch amplifier. Given that the SOA is regarded as a spatially concentrated device, it should be mentioned that the counterpropagating configuration of the MZI switch shown in Fig. 1 is just indicative, and the following theoretical analysis applies also to the copropagating configuration.

$G_1(t)$  is equal to  $G_2(t)$ , as given by (3), as long as no control signal is present, since we have regarded both SOAs as two identical devices. When a short optical control pulse with a power of  $P_{in}(t)$  is inserted into the upper branch SOA, the gain  $G_1(t)$  saturates below its steady-state value  $G_{CW}$  according to the expression [30], [31]

$$G_1(t) = \left[ 1 - \left( 1 - \frac{1}{G_{CW}} \right) \exp \left( - \int_{-\infty}^t P_{in}(t') dt' / U_{sat} \right) \right]^{-1}. \quad (4)$$

Hence, the time integral of  $P_{in}(t)$  represents the accumulated injected pulse energy and  $U_{sat}$  is the well-known saturation energy of the device. Equation (4) shows that the gain saturates to a minimum value until the whole pulse energy has passed through the semiconductor. From this time which we denote hereinafter as  $t_s$ , the gain recovers back to its steady-state value until the next control pulse enters the gate [31], with the stimulated carrier lifetime constant  $\tau_e$ . This constant is related to the SOA carrier lifetime  $\tau_c$  and the CW power level by  $\tau_e = \tau_c \tau_h / (\tau_c + \tau_h)$ , where  $\tau_h = U_{sat} / (P_{CW}/2)$ , relying on the principle of the optical holding beam technique [21].

For the case of intensity-modulated control pulse trains, the power of the  $k$ th individual control pulse can be expressed as

$$P_{in}^k(t) = P_0(1 + m \cdot \cos(\Omega \cdot k \cdot T)) \cdot a(t) \quad (5)$$

where  $a(t)$  represents the pulse waveform,  $P_0$  is the average peak power value across the whole control signal sequence,  $m$  is

the modulation depth index,  $\Omega$  is the modulation frequency, and  $T$  is the bit period. In what follows, the bit period is assumed to be greater than the stimulated carrier recombination time. This assumption can be valid even up to 40-Gb/s data rates, since current semiconductor technology can achieve carrier recovery times in the order of some picoseconds [32], which can be further reduced due to the presence of the strong CW signal [21]. In this way,  $G_1(t)$  will recover back to the initial  $G_{CW}$  value after each control pulse, allowing for the validity of (4) for the whole bit sequence. To this end, the switched waveform that appears at the S-port of the MZI gate is obtained by using (5), (4), (3), and (2) into (1), resulting in

$$P_S(t) = \frac{P_{CW}}{4} \left[ G_1(t) + G_{CW} - 2\sqrt{G_1(t)G_{CW}} \cdot \cos\left(-\frac{\alpha}{2} \cdot \ln \frac{G_1(t)}{G_{CW}}\right) \right] \quad (6)$$

where  $G_{CW}$  is given by (3) and  $G_1(t)$  is provided by

$$G_1(t) = \left[ 1 - \left(1 - \frac{1}{G_{CW}}\right) \cdot \exp\left(-\frac{P_0(1 + m \cos(\Omega k T)) \int_{-\infty}^t a(t') dt'}{U_{sat}}\right) \right]^{-1} \quad (7)$$

as the result of the insertion of (5) into (4).

Equations (6) and (7) provide a complete description of the interferometer's response to an injected intensity-modulated control pulse. In order to investigate the intensity modulation at the output of the gate, the calculation of the peak power of the switched pulse is required. Optimized switching performance is achieved when the average phase shift caused by the control pulses with  $P_0$  average peak power is  $\pi$ . Moreover, in order to avoid pulse-shape distortions in the switched signal, the maximum value of  $P_S(t)$  must temporally coincide with the minimum value of  $G_1(t)$  for every respective control pulse, which in turn corresponds to the moment  $t_s$ , where the whole

control pulse energy has been inserted into the SOA. This condition allows for the replacement of the time-dependent integral  $\int_{-\infty}^t a(t') dt'$  contained in (7) with a time-independent, constant value  $A$ , which represents the total area covered by the pulse waveform  $a(t)$ . This value corresponds to the limit of the integral at infinity. As a result, the peak power of the switched pulse is obtained by using (7) into (6), and it is only a function of the control pulse peak power  $P_0[1 + m \cdot \cos(\Omega \cdot k \cdot T)]$ , the  $G_{CW}$  value, and the saturation energy  $U_{sat}$ .

Expanding this switched pulse peak power expression into a Taylor series around the zero value of  $m$ , it can be written as a sum of a dc component, given by

$$\frac{P_{CW}}{4} \left[ G_1|_{m=0} + G_{CW} - 2\sqrt{G_1|_{m=0} \cdot G_{CW}} \cdot \cos\left(-\frac{\alpha}{2} \ln \frac{G_1|_{m=0}}{G_{CW}}\right) \right] \quad (8)$$

and an oscillating term at  $\Omega$ , given by (9), shown at the bottom of the page where the first derivative of  $G_1(m)$  is given by (10), shown at the bottom of the page.

By dividing the modulating power at  $\Omega$ , given by inserting (10) into (9), to the dc optical power, given by (8), the intensity modulation depth index  $m_{o/p}$  at the output of the gate can be obtained as (11), shown at the bottom of the page.

By applying the requirement for an average  $\pi$  phase shift to (2), the average minimum value of the gain is found to be  $G_1|_{m=0} = G_{CW} \cdot \exp(-2\pi/\alpha)$  and the required average optical control pulse power

$$\frac{U_{in}}{U_{sat}} = \frac{P_0 \cdot A}{U_{sat}} = \ln \frac{1 - \frac{1}{G_{CW}}}{1 - \frac{1}{G_{CW}} \cdot \exp\left(\frac{2\pi}{\alpha}\right)}. \quad (12)$$

Using the average minimum gain value expression, (10) and (12) into (11), the intensity modulation depth index at the output is expressed as

$$m_{o/p} = \frac{(1 + \exp(\frac{\pi}{\alpha})) \cdot \exp(-\frac{2\pi}{\alpha}) \cdot (1 - G_{CW} \cdot \exp(-\frac{2\pi}{\alpha}))}{1 + \exp(-\frac{2\pi}{\alpha}) + 2 \cdot \exp(-\frac{\pi}{\alpha})} \cdot \ln \left( \frac{1 - \frac{1}{G_{CW}}}{1 - \frac{1}{G_{CW}} \cdot \exp(\frac{2\pi}{\alpha})} \right) \cdot m. \quad (13)$$

---


$$\frac{P_{CW}}{4} \cdot m \cdot \frac{dG_1}{dm} \Big|_{m=0} \cdot \left\{ 1 - \sqrt{\frac{G_{CW}}{G_1|_{m=0}}} \left[ \cos\left(-\frac{\alpha}{2} \cdot \ln \frac{G_1|_{m=0}}{G_{CW}}\right) + \alpha \cdot \sin\left(-\frac{\alpha}{2} \cdot \ln \frac{G_1|_{m=0}}{G_{CW}}\right) \right] \right\}. \quad (9)$$


---

$$\frac{dG_1}{dm} \Big|_{m=0} = - \left[ 1 - \left(1 - \frac{1}{G_{CW}}\right) \exp\left(-\frac{P_0 \cdot A}{U_{sat}}\right) \right]^{-2} \left(1 - \frac{1}{G_{CW}}\right) \cdot \exp\left(-\frac{P_0 \cdot A}{U_{sat}}\right) \cdot \frac{P_0 \cdot A}{U_{sat}} \cdot \cos(\Omega \cdot k \cdot T). \quad (10)$$


---

$$m_{o/p} = \frac{m \cdot \frac{dG_1}{dm} \Big|_{m=0} \cdot \left\{ 1 - \sqrt{\frac{G_{CW}}{G_1|_{m=0}}} \left[ \cos\left(-\frac{\alpha}{2} \cdot \ln \frac{G_1|_{m=0}}{G_{CW}}\right) + \alpha \cdot \sin\left(-\frac{\alpha}{2} \cdot \ln \frac{G_1|_{m=0}}{G_{CW}}\right) \right] \right\}}{G_{CW} + G_1|_{m=0} - 2\sqrt{G_{CW} \cdot G_1|_{m=0}} \cdot \cos\left(-\frac{\alpha}{2} \ln \frac{G_1|_{m=0}}{G_{CW}}\right)}. \quad (11)$$

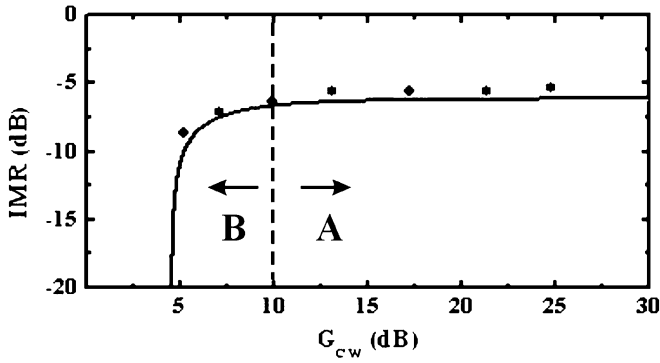


Fig. 2. Theoretically calculated (solid line) and experimentally measured (black dots) IMR at the output of the MZI gate for various  $G_{CW}$  values.

Equation (13) is the basic formula derived in this paper and provides the transfer function characteristics of the gate for the intensity modulating signal frequency components. It shows that the intensity modulation at the output is linearly related to the intensity modulation at the input and that the constant of proportionality depends on the gain  $G_{CW}$  and the linewidth enhancement factor of the SOA. Furthermore, this proportionality constant is less than 1, and the intensity modulation of the signal decreases at the output of the gate.

The IMR is defined as

$$IMR = 10 \cdot \log |m_{o/p}/m|. \quad (14)$$

Given that the intensity modulation depth indexes  $m$  and  $m_{o/p}$  of the control and the corresponding switched pulse sequence, respectively, are in principle the amplitudes of the slowly varying frequency component at  $\Omega$  that is responsible for the power fluctuations on the pulses, (14) denotes the amplitude suppression of this frequency component obtained at the output of the switch. More specifically, the  $m_{o/p}$  power level of the frequency component  $\Omega$  at the output of the gate will be reduced from its respective  $m$  power level at the input of the gate by an amount equal to the IMR value. To this end, (14) provides the frequency-domain transfer function of the gate with respect to the intensity modulating frequency components, for every possible saturation level of the SOA.

Fig. 2 shows the graphical representation of (14) for different values of  $G_{CW}$  in log scale, which in turn correspond to  $P_{CW}$  levels that can be calculated by making use of (3). It can be seen that when the SOA operates in the high-gain region A, corresponding to gain values between 10–30 dB, a nearly constant IMR of about 6 dB is obtained. However, as the gain decreases below 10 dB and the SOA is forced to operate in a low-gain region B of the graph, the IMR can exceed 10 dB. This reduction becomes even more pronounced as the  $G_{CW}$  value approaches the limit  $10 \cdot \log[\exp(2\pi/\alpha)]$ , which is dictated by the requirement for  $\pi$  phase shift. For the graph of Fig. 2 the linewidth enhancement factor  $\alpha$  was chosen to have a typical value of 6. Different values of  $\alpha$  would just change the  $G_{CW}$  limit and would simply shift the graph along the gain axis without altering its shape.

The discrimination between the two regions on the graph of Fig. 2 aims to provide a clear comparison between the properties of the SOA-based gate. Region A covers a broad SOA

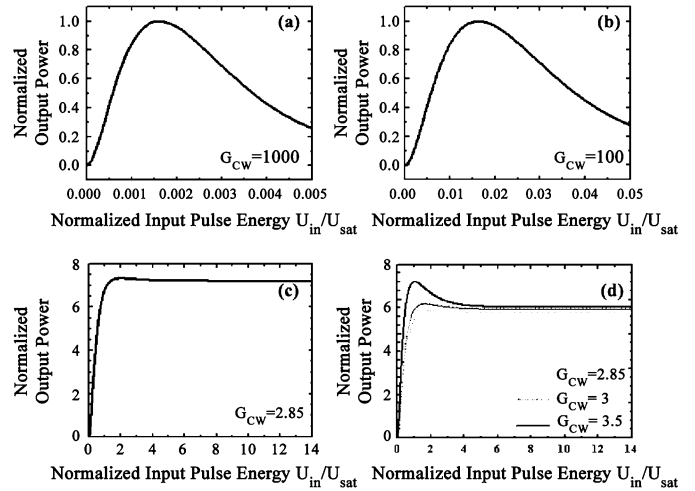


Fig. 3. Graphical representation of the theoretically calculated output-versus-input-power transfer function of the MZI gate for various  $G_{CW}$  values.

operational range, corresponds to the low or moderate saturation regime of the SOA, and is the region usually employed in switching schemes up to now. In contrast, region B is narrower, corresponds to the heavy saturation regime of the SOA, and offers enhanced intensity modulation suppression at the output of the gate.

In order to appreciate this behavior of optical gates in a better way, it is useful to investigate the output-versus-input-power transfer function of the interferometer for different  $G_{CW}$  values. This transfer function is obtained by inserting (7) into (6), neglecting the oscillating term at  $\Omega$  forcing  $m$  to be zero, and replacing the integral with A. The graphical illustration of this transfer function for various  $G_{CW}$  values is shown in Fig. 3. Fig. 3(a) and (b) depicts the normalized output power of the gate for linear gains  $G_{CW} = 1000$  and  $G_{CW} = 100$ , respectively, both values lying within the operational regime indicated by region A in Fig. 2. These two graphs have almost the same, well-known near-sinusoidal form that is responsible for the 6-dB IMR. The normalized switching power increases with the control pulse energy up to its maximum value that corresponds to a  $\pi$  phase shift and then decreases since the phase shift becomes greater than  $\pi$ . The main difference between the two graphs is that different pulse energies are required for the switching operation.

However, as the value of  $G_{CW}$  approaches its linear gain limit of  $\exp(2\pi/\alpha)$ , the normalized switched power curve takes a strongly nonlinear form that is almost parallel to the  $x$  axis, as shown in Fig. 3(c) and (d). This corresponds to the case of operating the SOA in the saturated regime of region B in Fig. 2, providing low gain. In this case, the output power increases again with the control pulse energy until a  $\pi$  phase shift is obtained, but then greater control pulse energies cause again an almost  $\pi$  phase shift, since the semiconductor is forced to operate near the material transparency and does not allow for gain values lower than unity. Fig. 3(c) is plotted for a  $G_{CW}$  value of 2.85, while Fig. 3(d) illustrates the switched power for three  $G_{CW}$  values, namely 2.85, 3, and 3.5. For both figures, the linewidth enhancement factor was again 6, resulting in a linear gain limit of  $\exp(2\pi/6) \approx 2.848$ .

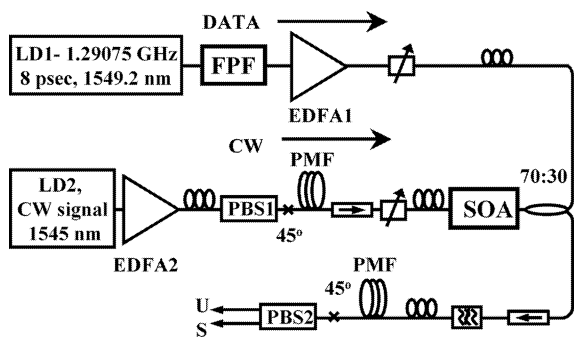


Fig. 4. Experimental setup.

The “flat” form that the switched power curve takes beyond a control pulse energy threshold explains the improved IMR properties of the gate, which may exceed 10 dB when the SOA is operated in the deeply saturated regime. However, this is achieved with control pulse energies much greater than those used in the cases described in Fig. 3(a) and (b). In Fig. 3(c) and (d), it is evident that control pulse energies greater than  $U_{\text{sat}}$  are required, and this is also dictated by (12).

### III. EXPERIMENT AND RESULTS

#### A. Experimental Transfer Function Derivation

The scope of this section is to provide experimental verification of the theoretically obtained “flat” transfer function. Fig. 4 shows the experimental setup used. A distributed feedback (DFB) laser diode (LD1), gain switched at 1.29075 GHz, was used to provide 8-ps pulses at 1549.2 nm, after linear compression. This clock stream was then inserted into a Fabry-Pérot filter (FPF) with a free spectral range (FSR) of 10.326 GHz and a finesse of 20.7. The role of the FPF was to fill the time intervals between consecutive 1.29075-GHz pulses with pulses at a repetition rate equal to the FSR of the filter, providing in this way a clock signal at 10.326 GHz with controllable intensity modulation. This pulse stream was then amplified in EDFA1 and launched via a 70:30 fiber coupler as the control signal into an UNI gate, powered by a CW signal at 1545 nm (LD2). The CW signal was amplified in EDFA2 and entered the UNI via the input polarization beam splitter (PBS1) to produce two orthogonal polarization components. The UNI gate was optimized for operation at 10.326 Gb/s and used polarization-maintaining fiber (PMF) at the input and output ports of the SOA to induce 50 ps of differential delay between the two orthogonal polarization components of the CW signal [29]. The active element was a 1.5-mm bulk InGaAsP/InP ridge waveguide SOA with 27-dB small-signal gain at 1550 nm, 24 dB at 1545 nm, 3-dB polarization gain dependence, and a recovery time of 100 ps, when driven with 700-mA dc current. After exiting the SOA, the polarization components of the CW signal were filtered in a 2-nm filter, had their relative delay removed, and were made to interfere in PBS2. The interferometer was biased so that, in the absence of the control signal, the CW signal appeared at its unswitched U-port while in the presence of the control it appeared at its switching S-port [3], [29]. Attenuators and polarization controllers were used in order to adjust the power level

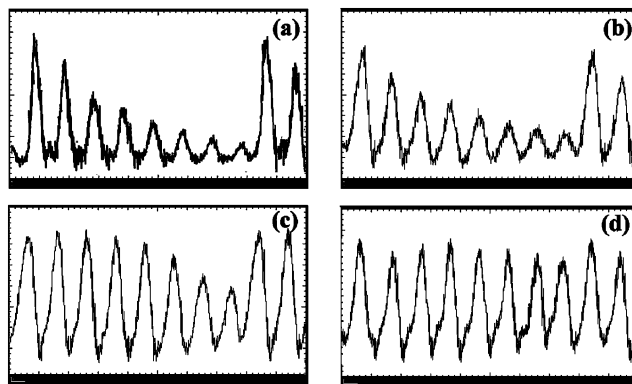


Fig. 5. (a) Control pulse sequence at the output of the FPF. (b)–(d) Corresponding switched pulse trains at the output of the gate for a control power of (b) 200  $\mu\text{W}$ , (c) 600  $\mu\text{W}$ , and (d) 800  $\mu\text{W}$ . The time base is 100 ps/div.

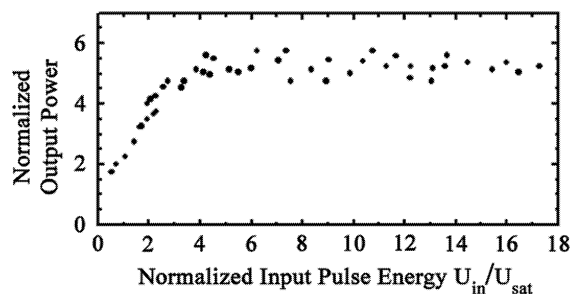


Fig. 6. Experimentally obtained transfer function of the UNI gate. The normalized output power is provided in arbitrary units.

and polarization states, respectively, of both the CW and control signals.

For the purposes of measurement, the SOA has to operate in the deeply saturated regime by means of strong CW input power level. After setting the SOA gain at the desired value, the energy of every switched pulse is measured and related to the corresponding control pulse energy. By repeating this procedure for various power levels of the injected control signal in order to cover the required range of control pulse energies, the output-versus-input-power transfer function is obtained.

Fig. 5(a) shows the control pulse sequence as it appears at the output of the FPF. The intensity modulation on these pulses has a period of 8 b, can be easily calculated as it originates from the memory properties of the filter, and has a maximum value of approximately 9 dB, if defined as the highest to the lowest pulse ratio. This provides a controllable way of measuring the energy of every individual pulse for a given average power of the control signal inserted into the SOA. Fig. 5(b)–(d) illustrates the corresponding switched signal for three indicative control signal powers inserted into the SOA, namely 200, 600, and 800  $\mu\text{W}$ , respectively. It is evident that the intensity modulation imposed on the switched pulses reduces to 7, 2.4, and 0.8 dB, respectively, as the control signal power increases. The CW power level that was used for saturating the SOA was 1 mW, and the  $U_{\text{sat}}$  parameter of the amplifier was found to be approximately 10 fJ.

Using the same CW power level, this measurement procedure was repeated for different control signal power values inside the SOA in order to cover a broad control pulse energy range. Fig. 6

shows the graphical representation of the experimentally obtained normalized output-versus-input-power transfer function, after correlating the output pulse energy to the respective control pulse energy for every injected control signal power. The output pulse peak power increases until it reaches a constant level, providing the expected “flat” transfer function. Comparison between Figs. 6 and 3(c) and (d) confirms the good agreement between theory and experiment. Minor variations between the two curves, like the  $U_{in}/U_{sat}$  threshold for obtaining the “flat” response, which is 3 in the experimentally obtained graph instead of the theoretically calculated one, are presumably due to the nonnegligible internal losses of the semiconductor.

The experimental setup of Fig. 4 was also used in order to experimentally verify the IMR graph shown in Fig. 2. By varying the CW power level inserted into the SOA in order to cover a broad operational SOA gain regime and by properly adjusting the control signal average power so as to obtain the optimum switching performance for every respective SOA steady-state gain, the intensity modulation of the switched pulse train, defined again as the highest to the lowest pulse ratio, was measured at the output of the gate. By calculating the difference between this value and the 9-dB intensity modulation of the initial control signal before entering the UNI gate, the experimental data for the IMR for every different SOA steady-state gain are obtained. These data are illustrated in Fig. 2 by the black dots, showing very good agreement between theory and experiment. For SOA gain values above 10 dB, the IMR was always approximately  $-5.5$  dB, whereas for a SOA steady-state gain equal to  $\sim 5$  dB, which is very close to the linear gain limit of 2.85, the experimentally obtained IMR was  $-8.2$  dB, as already mentioned before and confirmed by comparing Fig. 5(a) and (d). Although this measurement procedure was restricted by the FPF’s finesse that allowed for a maximum intensity modulation of 9 dB on the initial control pulses, the experimentally obtained data confirm the improved amplitude equalization properties of the gate as the SOA is driven into deeper saturation.

It should be mentioned that the use of a single SOA UNI gate for the experimental study instead of the dual SOA MZI gate of the theoretical analysis in Section II does not impair the conclusions of this study or the validity of the agreement, since both switches rely on the same principle of operation due to their interferometric arrangement. Moreover, in the present concept of IMR, the key parameter is the degree of saturation of the SOA, rather than the specific architecture of the interferometer. As such, the MZI configuration was chosen for the theoretical analysis for simplicity purposes. The same analysis for the UNI gate would require consideration of the nonlinear interaction between different polarization states inside the SOA, increasing the degree of complexity without offering additional information.

The most important assumption that has been made in the theoretical model concerns the SOA gain experienced by the CW input signal component that, in principle, should not be affected by the injected control signal. In the MZI structure shown in Fig. 1, the lower branch CW component has been assumed to perceive the steady-state SOA gain  $G_{CW}$ , whereas in the UNI gate, the time-delayed CW polarization component experiences the recovered SOA gain at a time instant of 50 ps after the con-

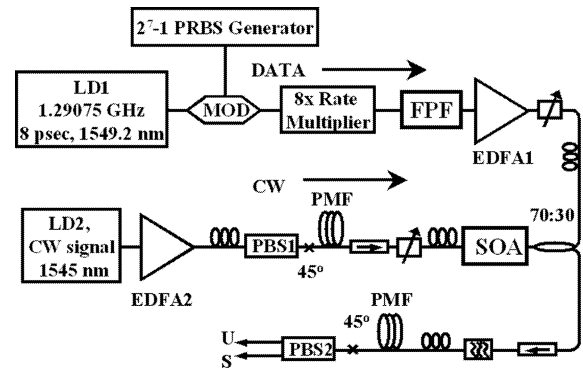


Fig. 7. Experimental setup.

trol pulse has passed through the SOA. However, this assumption does not affect the consistency between the theoretical and the experimental analysis when the SOA is biased in the deeply saturated regime, which is the region of prime interest in this paper, since in this case the recovered SOA gain experienced by the time-delayed polarization component in the UNI gate will be equal to the steady-state gain  $G_{CW}$ . In the saturated regime, the gain recovers back to its initial value with the stimulated carrier recovery time, which is much shorter than the corresponding small-signal gain recovery time and also shorter than 50 ps for the specific SOA used in the experiment, due to the injection of the strong CW signal [21].

### B. Performance Analysis With Random Modulation

In a real network system environment, optical pulse trains may suffer from a variable degree of intensity modulation, and in this section, we provide experimental data for the switch output in both the time and frequency domain for such cases.

The experimental setup used for this analysis is shown in Fig. 7. It is similar to the configuration used in part A of the same section and is depicted in Fig. 4, with some modifications for producing statistically random intensity modulation on the control signal. To this end, the 1.290 75-GHz clock pulse train provided directly by LD1 was modulated into a  $2^7 - 1$  pseudorandom bit sequence (PRBS) using a LiNbO<sub>3</sub> modulator driven by a PRBS generator. This data signal was launched into a fiber-based three-times bit interleaver and had its repetition rate multiplied by eight times, resulting in a 10.326-Gb/s pseudodata sequence. This sequence was then inserted into the FPF, producing in this way a randomly intensity-modulated clock pulse stream that was used as the control signal into the UNI gate. The FPF as well as the UNI gate arrangement were the same as in the experimental setup described in part A.

Fig. 8 illustrates the signal evolution as it propagates through the experimental configuration, both in the time and frequency domain. Fig. 8(a) displays a typical window of the produced 10.326-Gb/s data sequence, and Fig. 8(b) shows the corresponding electrical spectrum. At the FPF, the data stream is convolved with the exponentially decaying response function of the filter so that an intensity-modulated clock resembling signal is obtained, as illustrated in Fig. 8(c). For this time window, the imposed intensity modulation is approximately 9 dB. Fig. 8(d) shows the corresponding electrical spectrum at the output of the FPF where the data frequency components outside the 500-MHz

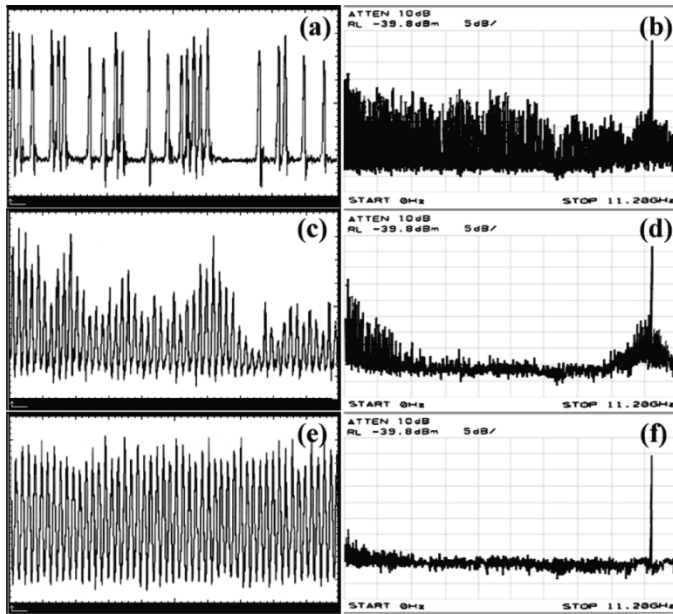


Fig. 8. Oscilloscope trace and electrical spectrum at the output of the (a) and (b)  $8\times$  rate multiplier, (c) and (d) Fabry-Pérot etalon, and (e) and (f) UNI optical gate. The time base of the oscilloscope traces is 500 ps/div. In the radio-frequency (RF) spectra, the span is from dc–11.2 GHz, and the amplitude scale is 5 dB/div.

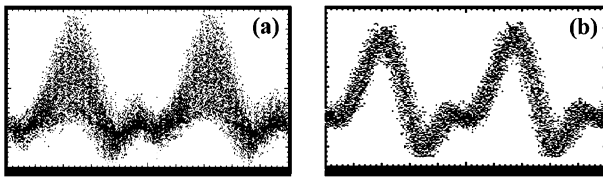


Fig. 9. Eye diagram of (a) the data pulses at the output of the FPF and (b) the switched pulses at the UNI output, respectively. Time base is 20 ps/div.

band of the filter have been suppressed. The imposed intensity modulation is due to the remaining data modes that remain within the filter band, around the 10.326-GHz clock component.

By inserting this intensity-modulated signal as control into the UNI, copolarized with one of the CW components in the SOA, a nearly equal amplitude clock pulse stream is obtained at the S-port. The switched output signal is depicted in Fig. 8(e), revealing an intensity modulation (highest to lowest pulse ratio) of less than 1.3 dB. The corresponding radio-frequency (RF) spectrum is shown in Fig. 8(f), where it is evident that all the intensity-modulating frequency components are suppressed in excess of 35 dB compared with the 10.326-GHz clock component. The switching power and mean energy per pulse for the CW and the control signal were 1 mW and 120 fJ, respectively.

Finally, in order to determine the quality of the switched signal at the output of the device, we have also performed eye measurements using a 30-GHz digital oscilloscope. Fig. 9 shows representative results, revealing the regenerative properties of the configuration. Fig. 9(a) illustrates the eye diagram of the incoming original data stream after their pass through the FPF. The severe intensity modulation on the data pulses arise from the memory properties of the filter (see also Fig. 8(c) and (d)) and result in a closed eye. The switched data at the output of the UNI are presented in Fig. 9(b), and its eye shows

significant improvement, revealing the increased amplitude equalization properties of the gate. The extinction ratio of the switched pulse sequence eye diagram was calculated, using the sampling oscilloscope, and was found to be 17 dB.

#### IV. DISCUSSION

The technique described here for IMR can provide enhanced performance characteristics to a variety of optical subsystems that incorporate interferometric gates. As an example, we can consider the configuration used in this paper for both the theoretical and experimental investigation of the IMR properties of the gate, which is actually a wavelength conversion device. In this scheme, the inserted control data stream is imprinted on the new wavelength provided by the CW signal that inputs the gate. Experimental demonstrations reported so far make use of wavelength converters either as data-routing elements [33] or as reamplification and reshaping (2R) regenerative devices [16]. The regenerative properties of SOA-based interferometric switches with the SOA operating in the small-signal gain regime clearly stem from the nonlinear sinusoidal transfer function of the gate. Within this frame, the described technique can definitely enhance the 2R regeneration capability of wavelength conversion devices as this can benefit from the endlessly nonlinear “flat” transfer function provided by the gate when the SOA is deeply saturated.

The increased tolerance to intensity-modulated control signals can also be useful to subsystems employing interferometric structures that require an optical clock pulse stream as the input signal. These subsystems mainly regard optical switching and signal processing applications, such as reamplification, reshaping, and retiming (3R) regeneration; demultiplexing; and Boolean logic functionalities. In these schemes, the CW signal can be considered as an additional third input optical beam whose role is to determine the operating regime of the switch. To this end, the clock input signal can be used as a low-input power probe beam that will perceive the gain and phase variations caused by the control signal. As a result, the switched clock pulses will exhibit the enhanced IMR capabilities of the gate. The separation of the CW and the clock signal at the output of the gate can be easily achieved by using different wavelengths for the two beams and a wavelength-selective filtering element.

Apart from the increased intensity equalization capabilities of saturated optical gates, the presence of the CW signal in principle provides improved signal-to-noise ratio for the switched signal, a very important parameter for the subsystems mentioned previously. The strong saturation of the SOA will limit the noise level imposed on the signal to be switched since it will reduce the amplified spontaneous emission (ASE) of the amplifier compared with the case where no CW beam is used.

Although this technique offers significant advantages to already adopted and demonstrated switching concepts, its importance becomes more pronounced in a recently demonstrated novel clock recovery device for optical packets [25]. This circuit achieves synchronization within a few bits on a packet-by-packet basis and can also operate in the asynchronous traffic regime requiring very small guard bands [26]. This configuration exploits the immediate response of a low finesse FPF for transforming the data packets into intensity-modulated packet clock signals and then employs a CW-powered optical gate for equalizing

the amplitudes of the packet clock pulses. This scheme clearly utilizes the switch capability to recognize and suppress the intensity-modulating frequency components, while the information carrying packet frequency harmonics remain unaffected, and the packet format of the extracted clock signal is retained. It should be noted that the packet clock recovery circuit has been the critical element in a variety of recently demonstrated novel optical subsystems for packet switching applications [27]–[29], highlighting the advantages offered by the presented technique to the interferometric structures.

## V. CONCLUSION

In conclusion, a detailed theoretical and experimental investigation of deeply saturated SOA-based interferometric gates has been demonstrated. Such devices have been shown to possess improved IMR properties. Analysis in the frequency domain revealed that the operation of the device in the deeply saturated regime provides increased IMR to RZ input data signals in excess of 10 dB, due to the almost flat, strongly nonlinear response. This concept has also been experimentally examined using 10-Gb/s pulse sequences with both periodical and random intensity modulation, and it has been shown that the experiment has verified the concept and its theoretical analysis. This scheme can be particularly applicable in several well-established switching and processing optical subsystems enhancing their performance characteristics or can even lead to novel functional subsystems for packet switching applications.

## REFERENCES

- [1] C. Bintjas, N. Pleros, and H. Avramopoulos, "System perspective for all-optical switching," in *IEEE/LEOS Newslett.*, vol. 16, Oct. 2002, pp. 19–21.
  - [2] M. Saruwatari, "All-optical signal processing for Terabit/second optical transmission," *IEEE J. Select. Topics Quantum Electron.*, vol. 6, pp. 1363–1374, Nov.–Dec. 2000.
  - [3] N. S. Patel, K. L. Hall, and K. A. Rauschenbach, "Interferometric all-optical switches for ultrafast signal processing," *Appl. Opt.*, vol. 37, pp. 2831–2842, May 1998.
  - [4] K. E. Stubkjaer, "Semiconductor optical amplifier-based all-optical gates for high-speed optical processing," *IEEE J. Select. Topics Quantum Electron.*, vol. 6, pp. 1428–1435, Nov.–Dec. 2000.
  - [5] B. Lavigne *et al.*, "Low input power all-optical 3R regenerator based on SOA devices for 42.66 Gbit/s ULH WDM RZ transmissions with 23 dB span loss and all-EDFA amplification," presented at the Optical Fiber Communication Conf. (OFC 2003), Atlanta, GA, 2003. PD15.
  - [6] M. Nakazawa, "Tb/s OTDM technology," in *Proc. European Conf. Optical Communication*, vol. 2, Amsterdam, The Netherlands, 2001, pp. 184–187. Tu.L.2.3.
  - [7] Y. Ueno, S. Nakamura, K. Tajima, and S. Kitamura, "3.8-THz wavelength conversion of picosecond pulses using a semiconductor delayed-interference signal-wavelength converter (DISC)," *IEEE Photon. Technol. Lett.*, vol. 10, pp. 346–348, Mar. 2002.
  - [8] K. L. Hall and K. A. Rauschenbach, "100 Gbit/s bitwise logic," *Opt. Lett.*, vol. 23, pp. 1271–1273, Aug. 1998.
  - [9] V. M. Menon *et al.*, "All-optical wavelength conversion using a regrowth-free monolithically integrated SAGNAC interferometer," *IEEE Photon. Technol. Lett.*, vol. 15, pp. 254–256, Feb. 2002.
  - [10] R. P. Webb, R. J. Manning, G. D. Maxwell, and A. J. Poustie, "40 Gbit/s all-optical XOR gate based on hybrid-integrated Mach-Zehnder interferometer," *Electron. Lett.*, vol. 39, pp. 79–81, Jan. 2003.
  - [11] C. Bintjas *et al.*, "20 Gbps all-optical XOR with UNI gate," *IEEE Photon. Technol. Lett.*, vol. 14, pp. 834–836, July 2000.
  - [12] C. Schubert *et al.*, "Comparison of interferometric all-optical switches for demultiplexing applications in high-speed OTDM systems," *J. Lightwave Technol.*, vol. 20, pp. 618–624, Apr. 2002.
  - [13] M. Tsurusawa, K. Nishimura, and M. Usami, "First demonstration of simultaneous demultiplexing from 80 Gb/s to 2 × 40 Gb/s by SOA-based all-optical polarization switch," in *Eur. Conf. Optical Communication*, vol. 4, Amsterdam, The Netherlands, 2001, pp. 500–501. Th.F.1.1.
  - [14] S. Nakamura, Y. Ueno, and K. Tajima, "168-Gb/s all-optical wavelength conversion with a symmetric-Mach-Zehnder-type switch," *IEEE Photon. Technol. Lett.*, vol. 13, pp. 1091–1093, Oct. 2001.
  - [15] M. L. Nielsen *et al.*, "40 Gbit/s standard-mode wavelength conversion in all-active MZI with very fast response," *Electron. Lett.*, vol. 39, pp. 385–386, Feb. 2003.
  - [16] A. E. Kelly *et al.*, "80-Gb/s all-optical regenerative wavelength conversion using semiconductor optical amplifier based interferometer," *Electron. Lett.*, vol. 35, pp. 1477–1478, Aug. 1999.
  - [17] O. Leclerc, "Optical 3R regeneration for 40 Gbit/s line-rates and beyond," in *Proc. Optical Fiber Communication Conf. (OFC 2002)*, 2002, pp. 79–81.
  - [18] C. Bornholdt, J. Slovak, and B. Sartorius, "Novel all-optical 3R regenerator concept demonstrated at 40 Gbit/s," presented at the Eur. Conf. Optical Communication, Copenhagen, Denmark, 2002. PD4.8.
  - [19] S. A. Hamilton and B. S. Robinson, "40-Gb/s all-optical packet synchronization and address comparison for OTDM networks," *IEEE Photon. Technol. Lett.*, vol. 14, pp. 209–211, Feb. 2002.
  - [20] H. J. S. Dorren *et al.*, "Optical packet switching and buffering by using all-optical signal processing methods," *J. Lightwave Technol.*, vol. 21, pp. 2–12, Jan. 2003.
  - [21] R. J. Manning and D. A. O. Davies, "Three-wavelength device for all-optical signal processing," *Opt. Lett.*, vol. 19, pp. 889–891, June 1994.
  - [22] M. Usami, M. Tsurusawa, and Y. Matsushima, "Mechanism for reducing recovery time of optical nonlinearity in semiconductor laser amplifier," *Appl. Phys. Lett.*, vol. 72, pp. 2657–2659, May 1998.
  - [23] J. L. Pleumeekers *et al.*, "Acceleration of gain recovery in semiconductor optical amplifiers by optical injection near transparency wavelength," *IEEE Photon. Technol. Lett.*, vol. 14, pp. 12–14, Jan. 2002.
  - [24] R. Inohara, K. Nishimura, M. Tsurusawa, and M. Usami, "Experimental analysis of cross-phase modulation and cross-gain modulation in SOA-injecting CW assist light," *IEEE Photon. Technol. Lett.*, vol. 15, pp. 1192–1194, Sept. 2003.
  - [25] C. Bintjas *et al.*, "Clock recovery circuit for optical packets," *IEEE Photon. Technol. Lett.*, vol. 14, pp. 1363–1365, Sept. 2002.
  - [26] N. Pleros *et al.*, "All-optical clock recovery from short, asynchronous data packets at 10 Gb/s," *IEEE Photon. Technol. Lett.*, vol. 15, pp. 1291–1293, Sept. 2003.
  - [27] C. Bintjas *et al.*, "All-optical packet address and payload separation," *IEEE Photon. Technol. Lett.*, vol. 14, pp. 1728–1730, Dec. 2002.
  - [28] G. T. Kanellos *et al.*, "Clock and data recovery circuit for 10 Gb/s asynchronous optical packets," *IEEE Photon. Technol. Lett.*, vol. 15, pp. 1666–1668, Nov. 2003.
  - [29] C. Bintjas, K. Vlachos, N. Pleros, and H. Avramopoulos, "Ultrafast nonlinear interferometer (UNI)-based digital optical circuits and their use in packet switching," *J. Lightwave Technol.* (Special Issue on Optical Networks), vol. 21, pp. 2629–2637, Nov. 2003.
  - [30] G. P. Agrawal and N. A. Olsson, "Self-phase modulation and spectral broadening of optical pulses in semiconductor laser amplifiers," *IEEE J. Quantum Electron.*, vol. 25, pp. 2297–2306, Nov. 1989.
  - [31] M. Eiselt, W. Pieper, and H. G. Weber, "SLALOM: Semiconductor laser amplifier in a loop mirror," *J. Lightwave Technol.*, vol. 13, pp. 2099–2112, Oct. 1995.
  - [32] T. Akiyama *et al.*, "Nonlinear gain dynamics in quantum-dot optical amplifiers and its application to optical communication devices," *IEEE J. Quantum Electron.*, vol. 37, pp. 1059–1065, Aug. 2001.
  - [33] C. Nuzman, J. Leuthold, R. Ryf, S. Chandrasekhar, C. R. Giles, and D. T. Neilson, "Design and implementation of wavelength-flexible network nodes," *J. Lightwave Technol.*, vol. 21, pp. 648–663, Mar. 2000.
- Nikos Pleros** (S'03), photograph and biography not available at the time of publication.
- Chris Bintjas**, photograph and biography not available at the time of publication.
- George T. Kanellos**, photograph and biography not available at the time of publication.
- Kyriakos Vlachos** (SM'98–M'02), photograph and biography not available at the time of publication.
- Hercules Avramopoulos**, photograph and biography not available at the time of publication.
- George Guekos** (S'66–M'69), photograph and biography not available at the time of publication.